Effect of the Electron−Phonon Interaction on the Luminescence Properties of Iron Ions in YAG Crystal

Pier Carlo Ricci,* Alberto Casu, and Alberto Anedda

Dipartimento Di Fisica-Università Di Cagliari, S.P N°8 Cagliari, Italy

Received: July 20, 2009; Revised Manuscript Received: September 29, 2009

High-resolution photoluminescence spectra of Fe:YAG crystals were recorded in the temperature range 10−150 K with different excitation energies, ranging from the band gap energy (6.88 eV) down to selective excitation of Fe^{3+} ions (2.40 eV). Iron levels fine structure is found in the zero phonon lines, whose characteristics hint at the presence of the doping Fe^{3+} ion in the tetrahedral site with a dynamic Jahn−Teller effect inherent in the $^4T_1$ excited states. The analysis of the zero phonon interactions with acoustic phonons was achieved through linear and quadratic electron−phonon coupling models, and the Huang−Rhys factor, the Debye temperature, and the electron−phonon coupling were calculated in the framework of the Debye approximation by including only the Raman two-phonon process. The interactions with lattice phonons were studied, and the results were found to be correspondent to the expected results from previous vibrational data.

Introduction

The zero-phonon line (ZPL) in the optical spectra of ions and atoms acting as percentually low dopants of solid matrices is a physical phenomenon interesting by itself but also useful for its possible applications as a tool of analysis, especially at low temperatures.[1−4] The quality of the informations that can be achieved through this method of measurement is obviously influenced by the degree of discernment of the physical phenomena related to the ZPL happening in concomitance with variations in temperature and the capability of relating the experimental data with the theory: the acquisition of high-resolution spectra is a necessary step to obtain a solid basis for an in-depth study of electron−phonon coupling (EPC). The choice of a widely known doped crystal is a logical way of trying to improve the use of ZPL as an analysis tool while trying to minimize possible problems of understanding the general outline.

Fe:YAG is a well-known doped crystal, and the contribution of the dopant to the performance of the host matrix has been an important field of research unto itself and in reference to YIG, where the Fe ion is part of the matrix instead of a dopant.[5−7] The studies on EPC of Fe^{3+} ions in a YAG matrix have been an important field of research in the past years to optimize the comprehension and the knowledge of various aspects such as the structure of energy levels and the role of optical centers in energy transfers for materials of interest in the fields of solid state lasers.[6,8]

The YAG crystal ($Y_2Al_5O_{12}$) (space group $Ia3d = O_h^{10}$) features Al^{3+} ions coordinated to nearest-neighboring oxygens with octahedral and tetrahedral point symmetry. The iron acts as a substitutional dopant for aluminum ions in the a and d sites with point symmetry Ga = 3 Ci and Gd = S_4, with octahedral and tetrahedral oxygen coordination, respectively. The larger radius of Fe^{3+} in comparison with that of Al^{3+} ion causes a variation in the local lattice structure and, consequently, an expansion distortion effect.[5,9]

This work is intended as a further step toward the full comprehension of the mechanics of EPC as a function of temperature through the study of the zero phonon line (ZPL) and vibronic sideband of Fe^{3+} doped YAG crystal providing an understanding of the thermal properties of spectral lines of ions in solids. The main goal is to obtain a full and unequivocal attribution of the transitions related to ZPL which, despite the amount of literature dedicated to the study and the analysis of the EPC, is still missing.

Experimental Section

Yttrium aluminum garnet samples were grown by SAES OPTO MATERIALS by the Czochralski method as provided by a research agreement with the University of Cagliari. Pure oxides of Al_2O_3 (99.999%) and Y_2O_3 (99.999%) were mixed and presintered under pressure of 140 MPa and processed at 1400 °C for 24 h. Sintered tablets were melted at 1970 °C in an iridium crucible and pulled at 0.8 mm/h with angular velocity $\omega_r = 15$ rpm under Ar^+ atmosphere. Samples were cut along the [111] direction and lapped to an optical finish.

Photoluminescence spectra of Fe:YAG crystals were recorded in two different rounds of measures, both collected with a temperature ramp and each one intended to enhance different aspects of the acquired data. The first round of measurements took place at the SUPERLUMI experimental station on the I beamline of the Hasylab synchrotron laboratories at DESY in Hamburg and allowed the collection of the whole luminescence spectra, thus taking into account the full vibronic sideband, although the observed ZPL did not seem to be fully resolved. The excitation was given by pulsed synchrotron radiation (SR), while the signal was dispersed by a 0.5 m Czerny−Turner monochromator and detected in the 1.5−5.0 eV energy range with a charge-coupled device (CCD). The emission spectral bandwidth was 0.1 nm. The spectra were recorded under multibunch operation and detected with an integral time window of 192 ns correlated to the SR pulses. A continuous-flow liquid-helium cryostat was used to vary the temperature of the sample chamber in the 10−150 K range.

The second round of measurements, operated with an Ar laser as the excitation source, was consequently devoted to obtaining high-resolution ZPL curves. The spectra were acquired with a

* Corresponding author. E-mail: carlo.ricci@dsf.unica.it.

10.1021/jp906864a CCC: $40.75
Published on Web 10/20/2009

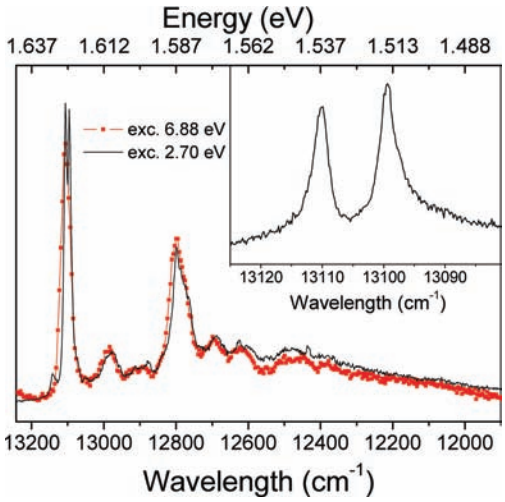

Figure 1. Photoluminescence spectra of Fe^{3+} ions in YAG crystal recorded at 10 K with excitation energy of 6.88 and 2.70 eV. The inset reports the high-resolution spectrum recorded at 10 K (excitation 2.70 eV) focused on the ZPL spectral region.

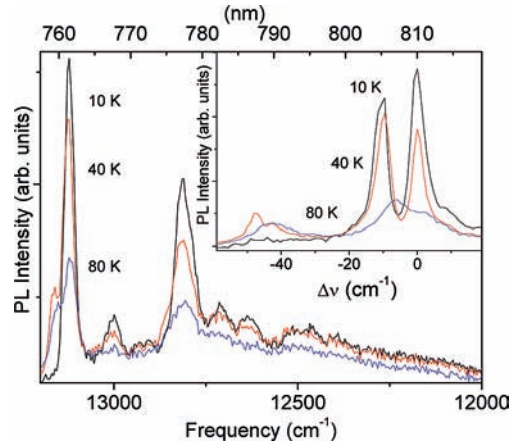

Figure 2. Photoluminescence spectra of Fe:YAG crystals as a function of sample temperatures. The inset reports the high-resolution spectrum (excitation 2.70 eV) focused on the ZPL spectral region.

triple spectrometer Jobin−Yvon Dilor integrated system with a spectral resolution of about 0.5 cm^{-1} and by a 1200 grooves/mm grating monochromator and a CCD detector system. During this round of measurements, the samples were mounted in an LTS-22-C-330 Workhorse-type optical cryogenic system for low-temperature measurements in the 10 ÷ 150 K range.

The Fe:YAG samples are commercial crystals grown by the Czochralski method, featuring a percentage of Fe doping of a few parts per million. The choice of such low quantity of dopant in the host matrix should be intended as a way of avoiding Fe−Fe interactions in favor of Fe−host interactions.

Results

The spectra were recorded on the basis of two different physical processes: the first set of measurements featured direct excitation of the host matrix with energy close to the band gap energy (at 6.88 eV), while measurements during the second set were performed with selective excitation of the Fe ions (whose absorption maxima are 3.04, 2.98, 2.70, and 2.62 eV).[10]

Figure 1 shows a PL spectrum recorded at 10 K. While the ZP line can be observed around 13 100 cm^{-1} (1.626 eV), the 12 797.1−12 766.1 cm^{-1} (1.588−1.584 eV) spectral range features the most complex structure of the spectrum, where the main system of the phonon repetition is reported: these bands derive from the transitions between the $^4T_1 \rightarrow {}^6A_1$ levels of Fe^{3+} ions.[8,10,11] No difference can be observed in the luminescence spectra from Fe ions dispersed in YAG crystals among the two sets of excitation energy, and for the sake of clarity, only the spectra at 10 K corresponding to an excitation of 6.88 and 2.70 eV are reported in Figure 1.

The inset of Figure 1 shows a high-resolution spectrum recorded at 10 K: the image highlights the result of resolving two ZPLs at 13 099.2 cm^{-1} (1.626 eV) (ZPL1) and 13 109.9 cm^{-1} (1.627 eV)(ZPL2), both featuring half-widths of less than 3 cm^{-1}, which improve the previous experimental results presented in ref 8. It is worth noting that ZPL1 features a quasi-Lorentzian peak profile with a slight asymmetry in the low-energy region, which could be ascribed to quadratic electron−phonon coupling.[12]

Figure 2 shows the emission spectra in the range between 12 000 and 13 200 cm^{-1} detected at different temperatures of the sample. Once again, the main part of the figure is devoted to show the variations in the characteristics of the overall spectra in a temperature ramp, while the inset is focused on the variations observed in the ZPLs, where the 0 value in the *x*-axis was chosen to clearly show the line shift. First of all, a different variation in intensity for ZPL2 and ZPL1 is clearly observable, so the ratio ZPL2/ZPL1 increases proportionally with the temperature and grows to a value higher than 1 already at 40 K. Besides, in the 40 K spectrum it is possible to observe the growth of a third hot line at 13 144 cm^{-1} (1.631 eV) (ZPL3) that seems to split in two components whose half-width, larger than the ones of ZPL1 and ZPL2, allows us to distinguish among them by only using two-Voigt profile fitting curves. The observation of four fine structure components of the $^4T_1(G)$ emission term in the luminescence spectrum allows us to determine the nature of the crystal field of the environment of the Fe^{3+} ions in the matrix by discriminating the coordination symmetry of the lattice position. Hence, the initial state of the emission degenerates at least in four components. The upper states are separated by 48 cm^{-1} from the lowest excited state.

If we look at the variations in the four ZPL components proportionally to the increase of temperature, three different processes can be pointed out. First of all, the intensity of the ZP lines decreases with the rising temperature, in conjunction with the enhancement of the phononic transition represented in the sideband, along with a broadening of the ZPLs and a shift toward lower energy. The temperature red shift observed in the ZPLs indicates the dominant role of electron−phonon interactions by comparison with thermal expansion of the lattice, which would have determined a blue shift.[13,14] The rise in temperature causes a decrease in the lifetime of the excited state of ZP transition, thus broadening the ZPLs, whose FWHM is inversely proportional to the aforementioned lifetime. Since the ZPL features both a Gaussian and a Lorentzian term, caused, respectively, by physical processes of random or equiprobable occurrence for each atom, the broadening of the lines must be considered as a Voigt-type process where the relative weight of the two components hints to the physical phenomena happening for each ZPL. It is clear to see a variation in the dependence of each ZPL on temperature in terms of intensity and peak shift: in particular, the lowest-energy peak features a higher dependence on temperature in terms of intensity and peak shift. The practical consequence of the simultaneous broadening and shifting of the peaks is that the main peaks overlap around 80 K, thus preventing them from physically deconvolving at higher temperatures.

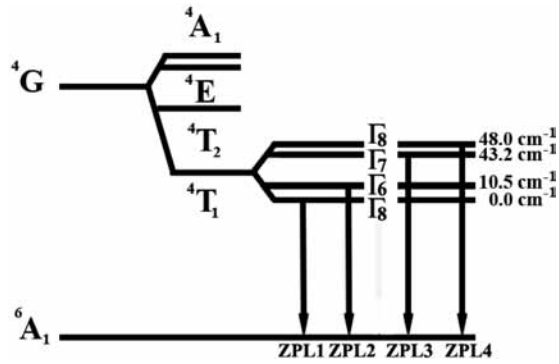

Figure 3. Level scheme of Fe^{3+} ion in a tetrahedral crystal field starting from the ^4G first excited state. The $^6A_1$ fundamental state is split into two additional states not resolved. For the observed ZP transition (ZPL1, ZPL2, ZPL3, and ZPL4) from the spin orbit coupling, four sublevels of the $^4T_1$ were indicated as well as their spacing from the fundamental transition.

The dependence on temperature of the coupling with optical phonons is also present, although its overall role is drastically reduced with respect to the ZPLs.

Discussion

The garnet crystals offer two sites for the transition ions, the octahedral a-site (of local C_{3i} symmetry) and the tetrahedral d-site (S4), the preference for substitution being determined by the mismatch of ionic radii of the dopant and host cation and on the electronic structure of the former. The d-sites show a better packing around the dodecahedral c-site (D_2 symmetry) occupied by the rare-earth ions, and the minimal d−c distance is shorter than the octahedral a−c distance.[11,15] The lowest spectral term of the ground electronic configuration $3d^5$ of Fe^{3+} is a spin sextet ^6S, while the excited states are spin quartets or doublets. This leads to the prohibition of transitions between the ground and excited states; however, the spin−orbit mixing of the sextet and quartet spin states increases the probability for sextet to quartet transitions: the corresponding levels are split by the cubic component of the crystal field according to the rules $^6S \rightarrow {}^6A_1$, $^4P \rightarrow {}^4T_1$, $^4D \rightarrow {}^4E + {}^4T_2$, $^4F \rightarrow {}^4A_2 + {}^4T_1 + {}^4T_2$, ^4G $^4A_1 + {}^4E + {}^4T_1 + {}^4T_2$, and the Tanabe−Sugano diagram, or the position of the crystal field levels as a function of the crystal field strength, is similar for octahedral and tetrahedral coordination.[16]

The crystal field strength D_q is generally at least twice as great for octahedrally coordinated ions with respect to tetrahedrally coordinated ions, and therefore, the $^4T_{1g}(^4G)$ and $^4T_{2g}(^4G)$ states will occur at lower energies than the $^4T_1(^4G)$ and $^4T_2(^4G)$ levels.[11,16] In opposition with tetrahedral sites, transitions to octahedral states should also be distinguishable on intensity grounds since the octahedral (or 3) symmetry causes transitions between $^6A_{1g}(^6S)$ and any of the 4G manifold to be parity forbidden. The lack of inversion at the tetrahedral site allows static mixing of higher energy, high intensity, odd parity transitions into the ground state. Consequently, transitions between the $^6A_1(^6S)$ ground state and the quartet excited states, being only spin forbidden, should exhibit higher intensity than those between $^6A_{1g}(^6S)$ and the excited quartet levels. Thus, in the case of the isolated Fe^{3+} centers in diluted garnets. the optical spectra will be dominated by the tetrahedral centers.

Figure 3 shows the crystal field states of a $3d^5$ electron configuration in a tetrahedral environment as it applies to the Fe^{3+} ion YAG crystal. The $^6A_1$ ground state of Fe^{3+} ($L = 0$, $S = 5/2$) is split into two states (Γ_8 and Γ_7) which are separated by less than 1 cm^{-1} (not resolved).[17] The ^4G first excited state splits by the T_d crystal field into four sublevels, where the lowest state is a $^4T_1$ level. In Figure 3, the higher excited states of the Fe^{3+} ion in a tetrahedral crystal field are also represented schematically. Additional spin−orbit coupling further splits the $^4T_1$ state into four sublevels, Γ_6, Γ_8, Γ_7, and Γ_8. According to crystal field theory, the states are separated by about 100 cm^{-1}. However, according to Koidl,[18] a dynamic Jahn−Teller effect can drastically reduce the pure crystal field splitting of the $^4T_1$ states. In the static limit, the four sublevels coincide in pairs [(Γ_8, T_7) and (Γ_6,Γ_8)]. Several $3d^5$ systems showing this behavior where the static Jahn−Teller limit is achieved are presented in the literature.[19,20]

The relatively strong and structured phonon replica and the fine structure of the ZPL reported in Figures 1 and 2 give evidence of a Jahn−Teller effect in the 13 100 cm^{-1} emission. For the present case, as can be observed in Figure 2, the $^4T_1$ state is split into four states, where the upper excited states are separated by 48.0, 43.2, and 10.5 cm^{-1} from the lowest $^4T_1$ level, respectively (inset of Figure 2 and Figure 3). From these experimental results, it is possible to affirm that the Jahn−Teller distortion does not reach the static limit for the Fe^{3+} ion in YAG crystals.

As previously pointed out in Figure 1, the ZPLs show a strong and structured phonon sideband, which consists on the one hand of broad bands due to coupling to lattice phonons and on the other hand of sharp lines due to coupling to defect-specific vibrational gap modes and vibrational resonant modes.

Besides the weak band at 25 cm^{-1} that can be attributed to the coupling to acoustic modes, the peaks observed in the vibronic part of the spectrum can be assigned to the coupling to optical (TO and LO) lattice phonons. The band at 12 993.3 cm^{-1} can be assigned to the overlapped contributions from 119 and 125 cm^{-1} optical modes (TO and LO, respectively). Other vibronics that can be assigned to the coupling with optical phonons can be revealed at 12 921.1 and 12 884.5 cm^{-1} relative to the TO and LO modes centered at 181 (LO) and 218 cm^{-1} (TO).[21]

The strongest coupling occurs for LO-type modes, and the most intense peak at 12 803.7 cm^{-1} has an energy distance of 298 cm^{-1} from ZPL1, coincident with the value of the LO modes derived by Hurrell at al.[21] Moreover, according to Papagelis et al.[22] the phonon density of states for garnet structures presents the maximum at about 300 cm^{-1}. For higher frequencies, the phonon density drops to zero, which means that following the Debye model it is possible to define the phonon cutoff frequency to 298 cm^{-1}.

In the range between 12 430 and 12 460 cm^{-1} we observe the coupling of the ZPLs to a series of very sharp phonons. These peaks reveal small half-widths (about 2 cm^{-1}) with respect to the phonon modes and different excitation spectra between them: the band at 12 435.1 cm^{-1} is always present in all the excitation spectra explored (6.88−2.40 eV), while the couple at 12 462.1 and at 12 456.9 cm^{-1} presents very sharp excitation spectra (2.72−2.66 eV) peaked at 2.69 eV in coincidence with the $^6A_1 \rightarrow {}^2T_2$ transition with a temperature-dependent behavior.[23] The first of these peaks can be attributed to iron-defect specific modes, while the twin peaks can be due to zero phonon recombination from $^2T_2$ to the first excited state $^4T_1$.

Different information on the coupling parameters of iron ions dispersed in the YAG crystal can be achieved from the study of the luminescence spectra in the 13 050−13 200 cm^{-1} spectral range as a function of temperature (Figure 2).

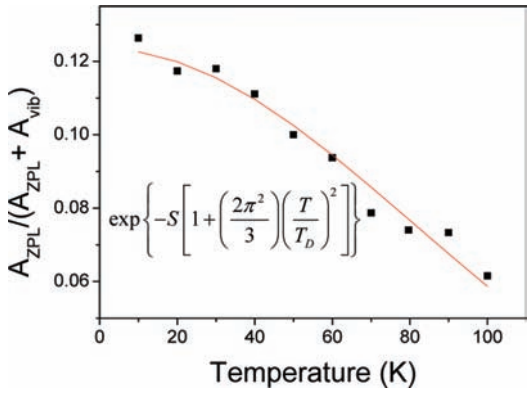

Figure 4. Experimental data of the ratio between the integrated area of the ZPL and the whole emission spectrum as a function of temperature. The solid curve represents the best fit curve according to the expression indicated and valid in the limit of $T \ll T_D$ (expression 3 in the text).

The behavior of the ZPL, intensity, line width, and asymmetric line shape is temperature dependent for systems having both linear and considerable quadratic interaction terms.

In the linear approximation of phonon coupling interactions, at $T = 0$ K and $p = 0$, phonons are not involved in the transition, and only the $n = 0$ vibrational state is occupied; the ZPL has the intensity[13]

$$I_{k=0}(T_{0K}, E) \propto e^{-S}\delta(\Delta E - E) \tag{1}$$

where ΔE is the energy of the zero phonon transition.

Besides the zero phonon line, there are also transitions that correspond to a change in phonon state of the lattice ($p \neq 0$). These multiphonon transitions will lead to the appearance of the broad phonon sideband, bounded to the ZPL in the low-temperature limit through the Huang−Rhys parameter S

$$\frac{I_1}{I_2} \cong e^{-S} \tag{2}$$

where I_1 and I_2 are the integrated area of the ZPL and multiphonon transition, respectively.

The basic feature at finite temperature of the ZPL and the multiphonon transition can be explained in the framework of the Debye approximation[8,14]

$$\frac{I_1}{I_2} = \frac{A_{ZPL}}{A_{ZPL} + A_{MP}} = \exp\left\{-S\left[1 + 4\left(\frac{T}{T_D}\right)^2 \int_0^{T_D/T} \frac{x}{e^x - 1}dx\right]\right\} \cong \exp\left\{-S\left[1 + \left(\frac{2\pi^2}{3}\right)\left(\frac{T}{T_D}\right)^2\right]\right\} \tag{3}$$

where T_D indicates the Debye temperature and S, the Huang−Rhys factor, represents the electron phonon strength of the system.

The expression 3, valid in the limit of $T \ll T_D$, well reproduces the experimental dependence of the ratio between the integrated area of the ZPL and the whole spectrum of the multiphonon transitions as a function of temperature (Figure 4). Considering that the fundamental ZPL transition at 13 099.2 cm^{-1} populates by thermal energy all the $^2T_2$ levels, it is worth noting that for ZPL intensity we have considered all the zero phonon transitions. The results of the fitting process ($S = 2.1$) confirm a medium coupling strength of the Fe ions in YAG crystals, and the value of the Debye temperature $T = 430$ K is in agreement with previous results.[8]

The increased spectral resolution of the second round of measurements allows a detailed analysis on the line width of the ZPLs to account for the physical processes contributing to the line shape. The homogeneous width of the ZPL is determined by the relaxation time T_2 of the excited electronic state of the ion and can be estimated as

$$\Gamma = \frac{1}{T_{2\partial}} = \frac{1}{T_1} + \frac{1}{T_2'} \tag{4}$$

where T_1 is the population relaxation time and T_2' is the pure dephasing time, determined by the fluctuations in the optical transition frequency. The anharmonic decay of the final vibrational state along with the decay of the initial electronic state are responsible for the residual homogeneous ZPL width observed in the limit of $T \rightarrow 0$, which means that a nearly constant inhomogeneous contribution, caused by strain and defects randomly distributed in the host lattice, should be considered in all the temperature ranges. It should be analytically expressed by a Gaussian curve, while the homogeneous components are represented by Lorentzian profiles. In the case both types of broadening processes are present, the line shape becomes the convolution of Lorentzian and Gaussian contributions: on the basis of the aforementioned considerations, the total analytical reconstruction of the experimental spectra was performed by means of Voigt profiles[24]

$$y = \frac{a_0 a_3}{2\pi\sqrt{\pi}a_2^2} \int_{-\infty}^{+\infty} \frac{\exp(-t^2)}{\frac{a_3^2}{2a^2} + \left(\frac{x - a_1}{\sqrt{2}a_2} - t\right)^2} dt \tag{5}$$

where a_0 and a_1 are the area and the center of the Voigt curve, while a_2 and a_3 are the weight of the Gaussian and Lorentzian component, respectively, corresponding to half-width at half-maximum of a pure Gaussian and a pure Lorentzian curve. However, it is worth noting that the ZPL1 line (Figure 1, inset) presents a nearly Lorentzian contour with a small asymmetry toward lower frequencies. These effects were previously noted in other samples with low concentration of dopants ($<10^{18}$ cm^3) in high-quality samples and reflect a very fine detail of the dopant−lattice interaction.[12] Generally, these effects are not counted for in the ZPL models and can be attributed to anharmonic contribution of the vibrations.

The rise in temperature leads to a broadening of the line widths caused predominantly by the interactions between electrons and acoustic phonons. Actually, the initial electronic state lifetime is almost constant in the temperature range examined (<150 K), and therefore the observed dependence was related to the dephasing effect in the curves of potential energy for the ground and excited states, resulting from an additional quadratic term in the electron−phonon coupling for each vibronic band.

The expression of the dependence of the line width from the temperature contains mainly the contributions from the natural line width (which is temperature independent), the one-phonon direct process Γ^D, the Raman two-phonon process Γ^R, and the radiative transition Γ^{rad} [24,25]

$$\Gamma(T) = \Gamma_{0K}^{inh} + \Gamma^{D} + \Gamma^{R} + \Delta\Gamma^{rad} \quad (6)$$

However, not all these contributions have the same weight as the temperature increases, and often they are not detectable in the analysis and can be neglected. The main contribution arises from the Raman two-phonon process, and using the Debye model of phonon energies, as temperature increases the interactions between electrons and acoustic phonons result in a line width broadening $\Delta\Gamma$, described by[24,25]

$$\Delta\Gamma^{R}(T) = \frac{k_b T_D}{\hbar}\frac{9}{4}\left(\frac{\omega}{\omega+1}\right)^2\left(\frac{T}{T_D}\right)^7 \int_0^{T_D/T} \frac{x^6 e^x}{(e^x-1)^2}dx \quad (7)$$

where ω is the quadratic coupling constant and T_D is the Debye temperature.

Since the line width caused by radiative decay is very narrow, and the probability of direct processes is small at low temperature, it is reasonable to assume that the contribution from the Raman process is the main part of the Lorentzian component of the ZPL. Crystal defects such as dislocations and point defects such as color centers are randomly distributed in the crystal and affect the electronic transition.

As previously discussed, and evidenced in Figure 5a, only the Lorentzian component needs to be taken into account for the deconvolution process. Although the analysis was conducted in a narrow range of temperatures (between 10 and 80 K, where the two components are still distinguishable), the fitting curves well reflect the experimental results, revealing a stronger coupling for the high-energy component (ZPL2).

The line shift as a function of temperature $\delta\nu$ also depends on the electron−phonon coupling strength and is determined by several contributions, such as the one-phonon or Orbach process. Since the peak position of the ZPL is independent of excitation energy, the contribution to the shift from localized modes may be neglected, and similarly to the line broadening case, the main contribution arises from the Raman two-phonon process.[24,25]

$$\delta\nu = \frac{k_b T_D}{\hbar}\frac{3}{4\pi}\frac{\omega}{\omega+1}\left(\frac{T}{T_D}\right)^4 \int_0^{T_D/T} \frac{x^3}{e^x-1}dx \quad (8)$$

Figure 5a and 5b reports the broadening (full width at half-maximum) and line shift of the two main ZP lines (ZPL1 and ZPL2) of Fe ions in YAG crystal as a function of temperature with respect to the values measured for the minimum temperature reached. The figures report the best fit of the experimental results using the quadratic coupling constant ϖ and the Debye temperature as free parameters in eqs 7 and 8. The capability of resolving two components allows the observation of two different behaviors in the ZPLs with varying temperature. For both fitting curves, a value of 450 K of the Debye temperature was found, but the ZPL component at higher energy (ZPL2) shows a heavier dependence from temperature, reflected by a higher coupling constant with respect to the value found for the ZPL1 line (−0.79 and −0.90, respectively). On the other hand, a distinct analysis of the two components can be performed only up to 80 K because the two bands are totally overlapped for higher temperatures and the deconvolution process loses its physical meaning. It is worth noting that the results obtained during these measurements are in agreement with the analysis previously performed on the not resolved spectra, which supplied a value of the coupling constant (−0.85) that seems to average the new results.[8]

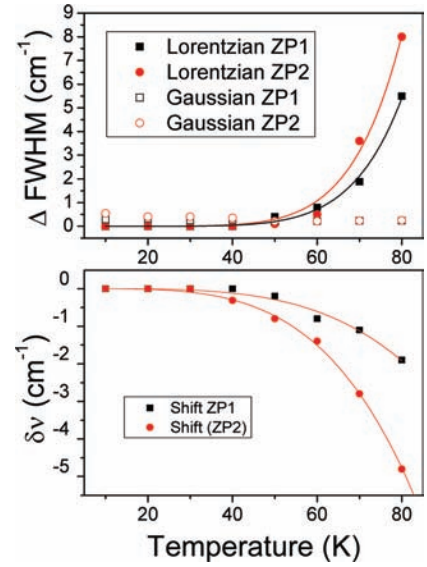

Figure 5. (A) Lorentzian and Gaussian component width of the two main zero phonon lines (ZPL1 and ZPL2) as a function of temperature obtained from analytical reconstruction using a Voigt profile. (B) Line shift of the two main zero phonon lines (ZP1 and ZP2) as a function of temperature. The solid lines reproduce the best fit results according to the Raman two-phonon contribution (expressions 7 and 8). For the line broadening, only the Lorentzian component was taken into account.

The analysis accomplished on the line broadening confirms a stronger coupling for the high-energy component. Moreover, the fitting results give a lower value of the coupling constant with respect to the analysis on the line shift (−0.73 and −0.78): this result should probably be addressed to the arbitrariness in the deconvolution process for higher-energy spectra; nonetheless, the results are sensibly more homogeneous with respect to the previous achievements.

Conclusions

PL spectra of Fe:YAG crystals were recorded in the temperature range 10−150 K with different excitation energies, ranging from the band gap energy (6.88 eV) down to selective excitation of Fe^{3+} ions (2.40 eV), the latter being acquired with a higher resolution to better observe the zero phonon optical transitions from Fe^{3+} levels. Low-temperature, high-resolution spectra led to identify four zero phonon lines, whose characteristics pointed toward the presence of the doping Fe^{3+} ion in the tetrahedral site with a dynamic Jahn−Teller effect inherent in the $^4T_1$ excited states. The interactions with lattice phonons were studied, and the results were found to be correspondent to the expected results from previous vibrational data. The analysis of the zero phonon interactions with acoustic phonons was achieved through linear and quadratic electron−phonon coupling models in the framework of the Debye approximation, and a good agreement between theoretical and experimental data was achieved by including only the Raman two-phonon process. According to these results, the analytical reconstruction of the zero phonon spectral profiles with Voigt function reveals a temperature-dependent behavior only for the Lorentzian contribution, while the inhomogenous broadening is nearly constant.

The study of zero phonon lines in high-resolution PL spectra of Fe:YAG crystals has once again shown the usefulness of this "tool", which proved to be capable of giving a new and unequivocal insight of the electronic transitions in the levels of the iron ion.

Acknowledgment. This work was supported by the European Community - Research Infrastructure Action under the FP6 "Structuring the European Research Area" Programme (through the Integrated Infrastructure Initiative "Integrating Activity on Synchrotron and Free-Electron-Laser Science").

References and Notes

(1) Zyubin, A. S.; Mebel, A. M.; Hayashi, M.; Chang, H. C.; Lin, S. H. *J. Phys. Chem. C* **2009**, *113*, 10432.

(2) Mahlik, S.; Grinberg, M.; Shi, L.; Seo, H. J. *J. Phys.: Condens. Matter* **2009**, *21*, 235603.

(3) Bachmann, V.; Ronda, C.; Meijerink, A. *Chem. Mater.* **2009**, *21*, 2077.

(4) Santos, J. R.; Vasilevskiy, M. I.; Filonovich, S. A. *Phys. Rev. B* **2008**, *78*, 245422.

(5) Dong, D.; Xiao-Yu, K.; Jian-Jun, G.; Hui, W.; Kang-Wei, Z. *Phys. Rev. B* **2005**, *72*, 073101.

(6) Rotman, S. R.; Warde, C.; Tuller, H. L.; Haggerty, J. *J. Appl. Phys* **1989**, *66*, 3207.

(7) Chen, Y. F.; Wu, K. T.; Yao, Y. D.; Peng, C. H.; You, K. L.; Tse, W. S. *Microelectr. Eng.* **2005**, *81*, 329.

(8) Anedda, A.; Carbonaro, C. M.; Chiriu, D.; Corpino, R.; Marceddu, M.; Ricci, P. C. *Phys. Rev. B* **2006**, *74*, 245108.

(9) Hurrell, J. P.; Porto, P. S.; ChNG, I. F.; Mitra, S. S.; Bauman, R. P. *Phys. Rev. B* **1968**, *173*, 851.

(10) Voitukevich, Y. A.; Korzhik, M. V.; Kuzmin, V. V.; Livshits, M. G.; Meilman, M. L. *Opt. Spectrosc.* **1987**, *63*, 810.

(11) Lupei, V.; Lupei, A.; Boulon, G.; Brenier, A.; Pedrini, C.; Elejalde, M. J. *Phys. Rev. B* **1994**, *49*, 7076.

(12) Sild, O.; Haller, K. *Zero Phonon Lines and Spectral Hole Burning in Spectroscopy and photochemistry*; Springer: Verlag Berlin Heidelberg, 1988; Chapters 3 and 4.

(13) Wang, H.; Medina, F. D.; Liu, D. D.; Zhous, Y. D. *J. Phys.: Condens. Matter* **1994**, *6*, 5373.

(14) Skinner, J. L.; Hsu, D. *Adv. Chem. Phys.* **1986**, *65*, 1.

(15) Roschmann, P. *J. Phys. Chem. Solids* **1980**, *41*, 569.

(16) Wemple, S. H.; Blank, S. L.; Seman, J. A.; Biolsi, W. A. *Phys. Rev. B* **1974**, *9*, 2134.

(17) Koschel, W. H.; Kaufmann, U.; Bishop, S. G. *Solid State Commun.* **1977**, *21*, 1069.

(18) Koidl, P. *Phys. Status Solidi B* **1976**, *74*, 477.

(19) Hoffman, A.; Anderson, F. G.; Weber, J. *Phys. Rev. B* **1990**, *41*, 5806.

(20) Pressel, K.; Bohnert, G.; Ruckert, G.; Thonke, K. *J. Appl. Phys.* **1992**, *71*, 5703.

(21) Hurrell, J. P.; Porto, P. S.; ChNG, I. F.; Mitra, S. S.; Bauman, R. P. *Phys. Rev. B* **1968**, *173*, 851.

(22) Papagelis, K.; Ves, S. *J. Appl. Phys.* **2003**, *94*, 6491.

(23) Voitukevich, Y. A.; Korzhik, M. V.; Kuzmin, V. V.; Livshits, M. G.; Meilman, M. L. *Opt. Spectrosc.* **1987**, *63*, 810.

(24) Powell, R. C. *Physics of Solid-State Laser Materials*; Springer-Verlag: New York, Inc., 1998; Chapters 4−5.

(25) Ellens, A.; Andres, H.; Meijerink, A.; Blasse, G. *Phys. Rev. B* **1997**, *55*, 173.

JP906864A